buildings

MDPI

Article

Study on the Synergistic Effect of Superabsorbent Polymer and Crystalline Admixture on Self-Healing Performance of Mortar Based on Image Binarization Method

Guang-Zhu Zhang [1], Xiang Ma [1] and Yao Liu [2,*]

[1] School of Civil Engineering and Transportation, Northeast Forestry University, Harbin 150040, China; zhangks@nefu.edu.cn (G.-Z.Z.); mx520038@nefu.edu.cn (X.M.)
[2] Department of Architectural Engineering, Kangwon National University, Chuncheon-si 24341, Republic of Korea
* Correspondence: lynefu@163.com

Abstract: Concrete self-healing technology is an effective method for autonomously repairing cracks, which can reduce the maintenance costs of concrete components and prolong their service life. This study investigates the mechanical properties and self-healing abilities of mortar with internally mixed superabsorbent polymers (SAPs) and crystalline admixtures (CAs). The compressive strength and recovery rate of the specimens were evaluated, and the self-healing performance of concrete specimens was assessed through water absorption tests and optical microscopy observation of healed cracks. Microscopic analysis of the crack fillings was conducted using SEM-EDS and XRD tests, revealing the mechanism of the synergistic effect of SAPs and CAs on self-healing. The results indicate that the physical filling effect of SAPs' water absorption and expansion almost completes the healing action before the 7-day healing age, with a weakened healing ability after this age. The chemical action of CA activation continues to heal cracks up to the 90-day healing age. When SAPs and CAs are incorporated together into the concrete matrix, the mortar specimens exhibit the best healing ability before the 7-day healing age. As water is released from the SAPs, the ongoing activation reaction of CAs shows the most effective healing result at the 90-day age. SEM-EDS analysis confirmed that the addition of CAs increases the Ca/Si ratio of calcium silicate hydrated, transforming it from an amorphous cluster structure to a needle-like structure. Furthermore, the internal curing effect of SAPs promotes the activation reaction of CAs, resulting in a greater quantity of more densely structured calcium silicate hydrated.

Keywords: crack; self-healing concrete; super absorbent polymers; crystallization admixture; mortars

Citation: Zhang, G.-Z.; Ma, X.; Liu, Y. Study on the Synergistic Effect of Superabsorbent Polymer and Crystalline Admixture on Self-Healing Performance of Mortar Based on Image Binarization Method. *Buildings* **2023**, *13*, 2953. https://doi.org/10.3390/buildings13122953

Academic Editor: Dan Bompa

Received: 4 November 2023
Revised: 22 November 2023
Accepted: 24 November 2023
Published: 27 November 2023

1. Introduction

Concrete, due to its low cost, moderate strength, and good durability, is widely used in the field of civil engineering [1]. However, concrete is prone to cracking under tensile stresses caused by external loads, shrinkage, temperature gradients, and expansion reactions [2]. To prolong the service life of concrete, manual repairs are often necessary, but this method can easily cause secondary cracking in the concrete [3]. Therefore, researchers have positively influenced the self-healing of concrete by incorporating methods such as hollow glass fibers [4], microcapsules [5,6], bacterial micro-organisms [7–9], and shape memory alloys (SMAs) [10,11]. Unfortunately, these methods have inherent challenges: the use of hollow glass fibers and microcapsule technology complicates on-site concrete pouring, bacterial micro-organisms struggle to survive in the highly alkaline environment inside concrete, and the high cost of SMA materials increases the construction cost of concrete structures.

Crystalline admixtures (CAs), as a unique type of permeability-reducing additive, are added to cement-based materials to decrease the permeability of concrete materials.

Al-Kheetan et al. [12] investigated the impact of introducing crystalline protective materials on the permeability of concrete. This study found that the depth of water penetration was 59 mm in concrete without crystalline materials, but reduced to 0 mm when crystalline materials were added, indicating an effective reduction in water permeability of concrete by the inclusion of crystalline materials. However, in recent years, researchers have attempted to improve the self-healing ability of concrete by adding permeable crystalline admixtures (CAs), which consist of particles of various sizes and chemical compositions. It is a hydrophilic and water-reactive permeable crystalline admixture [13]. CAs contain active chemical substances such as calcium oxide and silicon oxide, which can penetrate or disperse within the concrete structure with the help of water. Then, a part of these active substances reacts with the hydration products of cement [14] to form insoluble crystals, while other active substances promote the hydration of cement particles, thereby enhancing the healing ability and mechanical properties of cracked concrete [15]. Pejman and Azarsa et al. [13] studied the self-healing properties of concrete mixed with CAs. The study found that the addition of CAs reduces the porosity within the concrete, making its internal structure denser, and ultimately reducing the water penetration depth of the concrete by nearly 50%, indicating that the addition of CAs effectively improves the healing index in concrete specimens. Park et al. [16] studied the effect of CA addition on the healing of cracks in concrete specimens, using water flow tests and crack healing images to assess the specimens' healing ability. The experimental results showed that the cracks in the control specimens were not completely healed at 56 days, while the addition of CAs resulted in complete healing of the cracks in the concrete specimens at the 56-day healing age, indicating CAs' ability to self-heal cracks in concrete. However, researchers have found through extensive experimentation that CAs can heal cracks in cracked concrete, mainly due to the presence of water near the CAs. Roig-Flores et al. [17] studied the self-healing ability of concrete samples mixed with CAs under different curing environments. To evaluate the self-healing effect, permeability tests on cracked concrete were conducted. The study found that the healing index for specimens under submerged curing (fully submerged in water) and water contact curing (surface of the specimen immersed to a depth of 5 cm in water) were 93% and 81%, respectively, while the healing index for specimens under wet curing (humidity > 95%, temperature 20 ± 2 °C) and exposed to air curing were 21% and 17%, respectively. The experimental results indicate that CAs can exhibit optimal self-healing effects when sufficient water is present. Sisomphon et al. [14] studied the impact of the synergistic action of calcium sulfoaluminate-based expansive additives (CSAs) and CAs on the self-healing effect of cement-based materials. The results show that, due to the presence of water, mixtures containing CSAs and CAs have good surface crack healing capabilities, able to completely heal cracks up to about 400 μm. These studies demonstrate the crucial role of water in the CA-mediated healing process of concrete cracks.

Considering the important role of water in the CA-mediated healing of concrete cracks, the introduction of water-holding materials along with CAs can effectively enhance the self-healing effect of CAs. Zeolites [18], biochar [19], and superabsorbent polymers (SAP) are commonly used internal curing agents. Previous research has shown that SAPs are a cross-linked network of hydrophilic polymers capable of absorbing large amounts of water and eventually swelling into an insoluble gel, making it of greater research value; therefore, SAPs are considered a more ideal internal curing agent [20–24]. Due to the water-absorbing and swelling characteristics of SAPs, as well as its internal curing effect by releasing water within the concrete matrix, the water absorbed by SAPs can facilitate the healing of concrete cracks by CAs. Additionally, the insoluble gel formed by SAPs upon water absorption can serve to fill the cracks [25]. Yokota et al. [1] mixed fly ash with SAPs and incorporated it into concrete. They conducted repair experiments on the samples through continuous soaking and exposure to wet-dry conditions, finding that the synergistic effect of fly ash and SAPs enhances the self-healing ability of concrete. The width of the cracks decreased with the increasing substitution rate of fly ash, while the high content of SAPs reduced the crack width through the expansion of the gel, achieving up to 100% closure of cracks and

restoration of permeability in 28 days. Lee et al. [26] studied the effect of using SAPs on the self-healing of concrete cracks. They investigated the influence of SAP types, dosage, and crack width on the self-sealing efficiency of concrete through water permeability tests. They tested four different dosages of SAP types and full-thickness crack widths ranging from 0.1 mm to 0.4 mm. The water flow experiments revealed that the addition of SAPs reduced peak flow and cumulative flow by 85% and 98%, respectively, and sealed 0.3 mm cracks. Moreover, increasing the dosage of the SAPs significantly affected the acceleration of crack sealing and the reduction of total flow through the cracks. This demonstrates the feasibility of SAPs themselves as an additive for the self-sealing of concrete cracks. Snoeck et al. [27] used X-ray computed microtomography to study the self-healing of cementitious materials promoted by SAPs. They found that with the use of SAP particles, shallow regions about 800–1000 μm from the surface were completely healed. The healing products were $CaCO_3$, and a small portion of $Ca(OH)_2$ and C-S-H. Steuperaert et al. [28] visualized the water permeability of cement materials with SAPs using neutron radiography. They discovered that compared to the control, the capillary water absorption rate decreased after the addition of SAPs, and the permeability of cracked concrete also decreased. This is mainly attributed to the expansion of SAPs on the crack surfaces and the blockage of the cracks. SAPs have been proven effective when used alone as a self-healing agent in concrete, but research on their combined effect with CAs as a water-retaining material to improve concrete self-healing has yet to be found.

The study on the separate incorporation of CAs and SAPs into concrete for mechanical properties is very clear. The use of SAPs reduces the compressive strength, while the addition of CAs increases the compressive strength of concrete [29]. This is mainly due to the different reaction mechanisms of the two in cementitious materials. The active chemical substances in CAs, along with water, enter the concrete. The cement hydration process produces a large amount of $Ca(OH)_2$, and the active substances in CAs react with the $Ca(OH)_2$ formed during hydration, creating stable and water-insoluble calcium silicate hydrate that fills the pores of the concrete [30], effectively enhancing the mechanical properties of the concrete structure [31]. Azarsa et al. [13] studied the impact of incorporating CAs on the mechanical properties of concrete, testing the average compressive strength of specimens cured for 28 days. It was found that, after adding CAs, the compressive strength of the OPC mixture increased by 11%. However, tests on the mechanical properties of concrete mixed with SAPs revealed that SAPs significantly weaken these properties. Gruyaert et al. [32] used SAPs with a particle size of less than 400 μm in concrete mixtures, at 0.5% and 1% of the weight of the cement, and the results showed a general decrease in the compressive strength of all concrete with added SAPs. In another study, Geuntae Hong et al. [33] investigated the rapid self-healing of cracks in cementitious materials with SAPs, finding that the 28-day compressive strengths of Control, S-0.5, and S-1.0 samples were 45.8 MPa, 35.4 MPa, and 25.6 MPa, respectively; the compressive strengths of S-0.5 and S-1.0 were 77.3% and 55.9% of the Control sample, respectively. They confirmed that the compressive strength of the Control was higher than that of the mortar samples with added SAPs at different curing ages, as the addition of SAPs resulted in more porosity within the samples, reducing their compressive strength. D. Snoeck et al. [34] studied the effect of SAPs and additional water on the strength of mortar with a water-cement ratio of 0.50, finding that the addition of SAPs increased the large pores within the samples, which were irregular in shape, preventing the transmission of compressive loads through dome action, leading to lower compressive strength. The above studies have reported the individual use of SAPs and CAs on the mechanical properties of concrete, but the mechanism of their combined effect on concrete mechanical properties is not yet clear.

This paper investigates the effects of SAPs, CAs, and their combined action on the self-healing of cracks in cement mortar. Through mechanical performance tests, the compressive strength recovery rate, optical microscopy observations, and water absorption tests, the macroscopic self-healing properties of cracks were studied. Additionally, SEM and XRD micro-experiments were used to identify the fillers in the cracks, ultimately revealing the

mechanism of the combined effect of SAPs and CAs on the self-healing of mortar cracks. The innovations of this study include the following three aspects: First, the mechanism by which water promotes the activation reaction of CAs to enhance self-healing ability was clarified through crack observation tests and SEM-EDS experiments; Second, the micro-experiments revealed the mechanism of the effects of SAP water absorption and expansion, internal curing, and the CA activation reaction on the self-healing properties of cracks; Finally, the impact of SAPs, CAs, and the synergistic effect of SAPs and CAs on the healing index of cracks at different healing ages was clarified through crack healing tests.

2. Experimental Materials and Methods

2.1. Experimental Materials

The materials mainly used in this study include ordinary Portland cement (OPC) and standard fine sand, as well as crosslinked copolymer SAP composed of acrylamide and acrylic acid ester. The CA deployed was in powdered form. X-ray fluorescence (XRF) spectroscopy was utilized to determine the chemical composition of both OPC and CA powders, the results of which are tabulated in Table 1.

Table 1. Chemical compositions of OPC and CA powders (wt.%).

Material	Chemical Composition (Mass %)							
	CaO	SiO_2	Al_2O_3	Fe_2O_3	SO_3	MgO	Others	Loss on Ignition
OPC	64.14	18.55	4.41	3.23	3.03	2.04	2.07	2.53
CA	65.84	19.84	4.47	3.33	3.12	1.24	2.12	0.04

2.2. Mix Proportions and Specimen Preparation

Previous studies have shown that SAPs, being a highly absorbent polymer, release absorbed water during cement hydration, introducing additional porosity into the cement matrix, which reduces the strength of the specimens. When the addition of SAPs exceeds 0.5%, this trend of strength reduction becomes more pronounced [35]. Studies on adding CAs as a self-healing agent in the cement matrix indicate that maintaining the proportion of CAs at 4% not only improves the mechanical properties of the specimens but also enhances crack healing effects [36]. In summary, in the experimental process, SAP replaced 0.5% of the cement (by weight), while CA replaced 4% of the cement (by weight). Table 2 presents the mixing ratio design of four group mixtures used in this study. The concrete mortar without SAP and CA as the control group were labeled as Control. Mortar specimens with 0.5 wt.% SAP of cement added was labeled as 0.5SAP. Mortar specimens with 4 wt.% CA of cement added were labeled as 4CA. All mortar mixtures containing 0.5 wt.% SAP and 4 wt.% CA of cement were labeled as 0.5SAP4CA. The water–binders ratio for all mixtures was set to 0.5 (w/b = 0.5) and a sand–binders ratio of 2.0 (s/b = 2.0). During the mortar mixing process, SAP absorbs parts of free water because of the water absorption property. For all specimens with uniform flow properties, 0.07 wt.% superplasticizers of binders were added to the specimens mixed with SAP. All mortar specimens were cast into 50 mm × 50 mm × 50 mm sizes and the specific process of mortar preparation was implemented as followed steps: (1) Solid materials (OPC, CA, SAP, and standard sands) were proportionally added into a cement mortar mixer and stirred at low speed for 30 s. (2) Water and a polycarboxylate superplasticizer were mixed, and the mixture was then added to the mixing pot and stirred at low speed for 2 min. (3) Stirring was halted for 30 s, and a spatula was used to thoroughly mix the unmixed cement slurry at the bottom of the pot. (4) The slurry was additionally stirred at high speed for 3 min. All the mixed materials were then poured into molds and vibrated to ensure compaction. To maintain moisture, the specimens were covered with polyethylene film and demolded after curing for 24 h at room temperature (20 ± 1 °C), then placed in water (20 ± 1 °C) for curing.

Table 2. A mixed ratio of all specimens.

Mixture ID	Water (g)	Binders			W/B	Sand (g)	Superplasticizer (g)
		Cement (g)	SAP (g)	CA (g)			
Control	500	1000	-	-	0.5	2000	-
0.5SAP		995	5	-			0.7
4CA		960	-	40			-
0.5SAP4CA		955	5	40			0.7

For specimen pre-cracks, specimens cured in water for 3 days were positioned within YAW-300D microcomputer-controlled cement compression and flexure testing apparatus. Figure 1 shows schematic diagram. In order to pre-crack the specimen with a width of 100–300 μm, a steel wire of approximately 1 mm diameter and 50 mm length is placed at bottom of specimen. A load was applied to the specimen, the loading rate was set to 0.5 KN/s, and the loading force value was set to 33 KN–43 KN until the target crack width was obtained. Figure 2a shows a schematic diagram of pre-cracks apparatus for mortar specimens, and Figure 2b demonstrates pre-cracked mortar specimens.

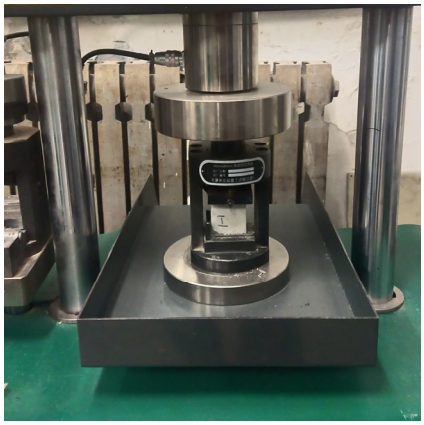

Figure 1. Crack treatment device.

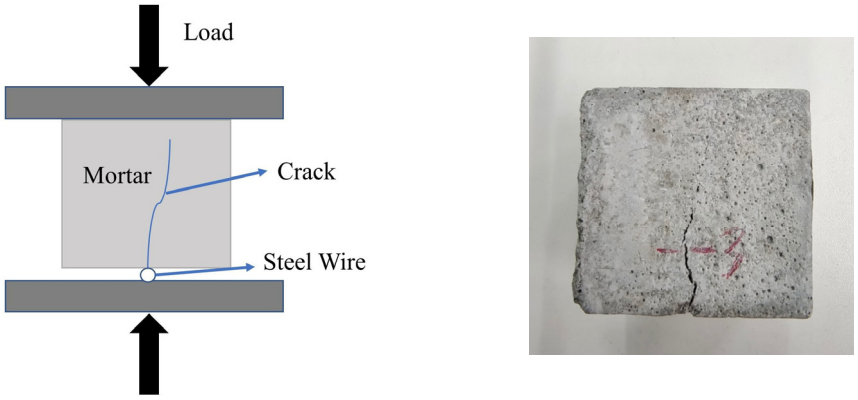

(**a**) (**b**)

Figure 2. (**a**) Schematic diagram of crack manufacture, and (**b**) pre-cracked mortar specimen.

2.3. Experimental Methods

2.3.1. Crack Healing Index

This study evaluates the self-healing performance of mortar by measuring the crack healing index. Cracks were observed using the OLYMPUS BX53M stereo microscope (Olympus Corporation, Tokyo, Japan) and measured and recorded using image analysis

software (Vistarimage—VQS300). The cracks' initial conditions (healing age of 0 days) and changes in cracks at healing ages of 7, 28, and 90 days were observed. The pixel resolution for each crack image was 640 × 480. Adobe Photoshop CS7 software was used for image binarization of captured results [37]. Figure 3 illustrates the results of image-processing analysis. Adobe Photoshop was employed to calculate the white areas (crack regions) and the healing index in the images. The crack healing index (η) was calculated using Formula (1):

$$\eta = \frac{A_0 - A_t}{A_0} \quad (1)$$

where η was the crack healing index (%); A_0 was the initial crack area (mm^2); and A_t was the crack area after healing for t days (mm^2).

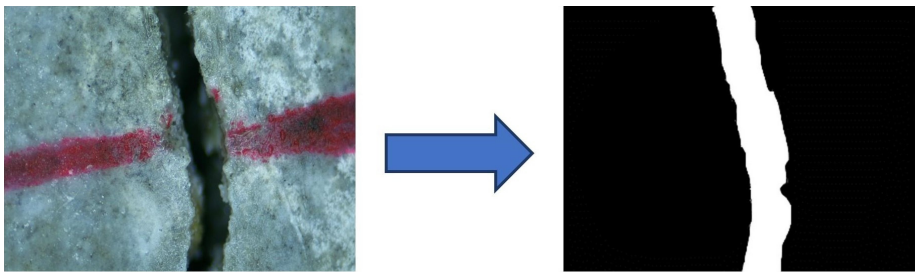

(**a**) (**b**)

Figure 3. Crack image-processing method: (**a**) Initial crack image, and (**b**) binarization of the output image.

2.3.2. Compressive Strength

When investigating the impact of the incorporation of SAPs and CAs on the mechanical properties of mortar, it is necessary to conduct compressive strength assessments in accordance with ASTM C109-21 standards [38]. These assessments were performed using the YAW-300D microcomputer-controlled equipment for cement compressive and flexural tests. Strength tests were conducted on three specimens within the same group, and the average of the three measured strengths was taken for compressive strength analysis.

2.3.3. Compressive Strength Recovery

In this experiment, the compressive strength of the specimens was tested at 28 days of curing, and then compressive strength recovery of the pre-cracked specimens was tested after healing at 28 days of age. The compressive strength recovery rate (R) was calculated as indicated in Equation (2) [39]:

$$R = \frac{f_t^{healed}}{f_t^{virgin}} \times 100\% \quad (2)$$

where f_t^{healed} was compressive strength recovery of pre-cracked specimens cured for t days of healing age (MPa), and f_t^{virgin} was compressive strength of specimens cured for t days of curing age (MPa).

2.3.4. Water Absorption Test

According to the ASTM C1585-20 [40] standard, water absorption tests were conducted on mortar specimens with a healing age of 28 days. Initially, the specimens were placed in an oven at a temperature of 50 ± 2 °C. Subsequently, epoxy resin was used to seal all four surfaces of each specimen (excluding the fracture surface and its counterpart). The fracture surfaces of each specimen were immersed in water by 5 mm. Finally, mass measurements were taken at predetermined time intervals (1, 5, 10, 20, 30, 60, 120, 180, 240, 300, and 360 min) using a precision electronic balance. Instrumentation used for

water absorption measurements is illustrated in Figure 4. The water absorption height was quantified according to Formula (3):

$$I = \frac{m_t}{A\rho} \tag{3}$$

where I was the water absorption height (mm); m_t was the mass of the specimen at t mins (g); A was the crack surface area (mm^2); and ρ was the density of water (g/mm^3).

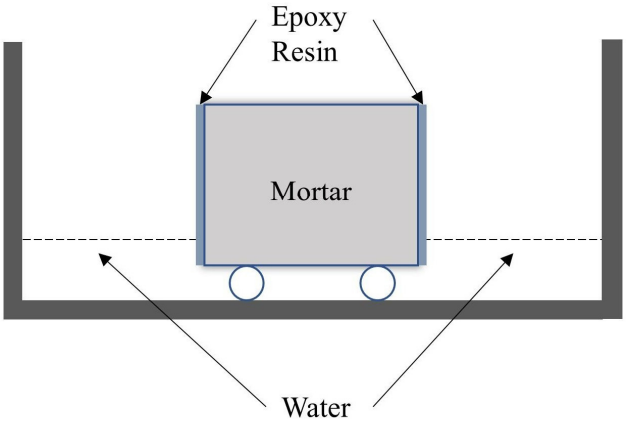

Figure 4. Water absorption test setup for mortar specimens.

2.3.5. Microstructure Analysis

(1) SEM-EDS test

The healing filler in the crack was removed by blade scraping, followed by drying at 40 °C in an oven for 24 h. The morphology of the filler at the crack was observed using a scanning electron microscope (SEM). Elemental analysis of the filler was conducted using energy dispersive spectroscopy (EDS). The testing equipment is illustrated in Figure 5. The imaging principle involves primary electrons generating low-energy secondary electrons, and high atomic number (Z) contrast images are produced through backscattering of primary electrons.

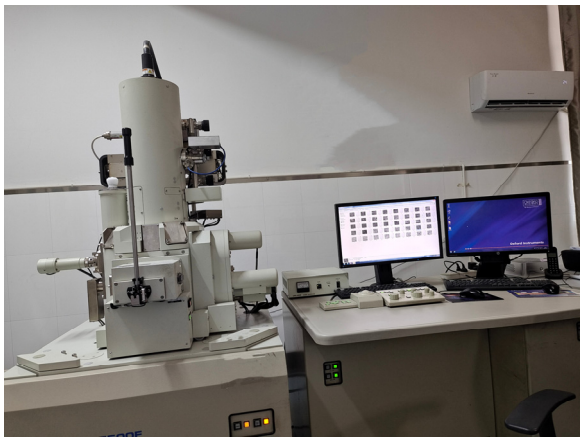

Figure 5. SEM-EDS test equipment.

(2) X-ray diffraction

To analyze the crystalline phase composition of the filler, XRD testing was performed using XRD-6100 (Shimadzu, Japan), and the specific results are shown in Figure 6. The filler was collected from the cracks of the sample using a blade, then dried in an oven at 40 °C for 24 h and ground into powder. Subsequently, the powder was sieved through a 200-mesh sieve and subjected to XRD testing. MDI Jade 6.5 software was employed to analyze the characteristic peaks of crystals in the filler. The samples were scanned using a

diffractometer with a copper anode, with a scanning range of 10° to 70° and an observation step of 0.02°. All experimental methods and procedures used in this study are illustrated in Figure 7.

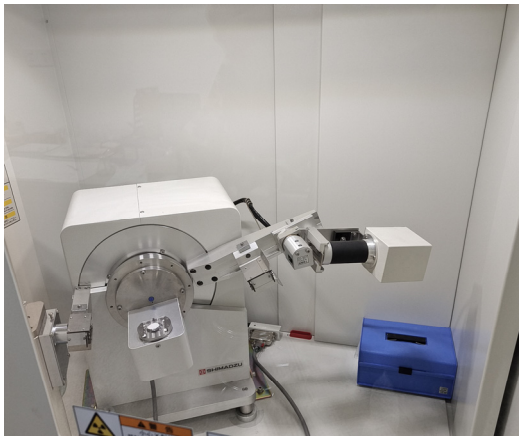

Figure 6. X-ray diffractometer.

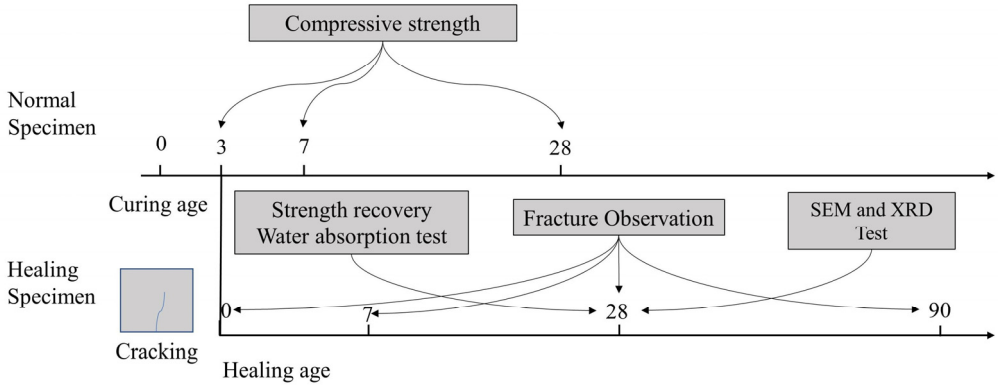

Figure 7. The specific process of experimental tests.

3. Results and Discussion

3.1. Crack Observation

The crack observation images of specimens are shown in Figure 8. The figure indicates that Control specimens had minimal impact on crack healing after 90 days. By contrast, the 0.5SAP, 4CA, and 0.5SAP4CA specimens exhibited pronounced healing effect compared to Control specimens.

For healing results at 7 days of healing age in Figure 8, 0.5SAP specimens show a more significant healing effect compared to the healing effect of the 4CA specimens. Figure 9 shows that 0.5SAP specimens had a crack healing index of 58.2%, while the crack healing index for 4CA specimens was 31.9%. The specific healing index is shown in Table 3. For 0.5SAP specimens, the cracks were plugged by the physical filling effect. This occurred as the SAP within the cracks imbibed water, subsequently swelling to form an insoluble gel material, which contributed to partial crack healing. And this physical filling effect is quickly demonstrated during the initial stages of crack healing. The crack healing in 4CA specimens can be attributed to the activating substance in CAs reacting with $Ca(OH)_2$. This reaction generates a dense hydrated calcium silicate that fills the cracks. The SEM-EDS and XRD tests have confirmed this conclusion. The healing time required for reaction products to fill the cracks was longer than that of the physical filling effect. Therefore, the utilization of the SAP to produce soft gels through water absorption and swelling demonstrates more pronounced effects than filling cracks by reaction products of activated substances in the CA at early ages. Snoeck D. et al. [41] reported similar experimental results. For the

0.5SAP4CA specimen, the healing index was 78.2% at 7 days, showing a more significant healing effect compared to the 0.5SAP and 4CA specimens. This is primarily due to three reasons: First, the SAP added to the 0.5SAP4CA specimens absorbs water and swells, forming an insoluble gel material that fills the cracks. Secondly, the active substances in the CA react with lime and oxides in the cement material, promoting the formation of ettringite crystals, which fill the cracks and lead to healing. Lastly, water can facilitate the reaction between the activating substances in the CA and the cement hydration products, forming more calcium hydrated silicate [42]. The water absorbed by the SAP is released as the cement continues to react, providing more water for the activation reaction in the CA, resulting in the formation of more calcium silicate hydrated. These reaction products will be confirmed in subsequent SEM images.

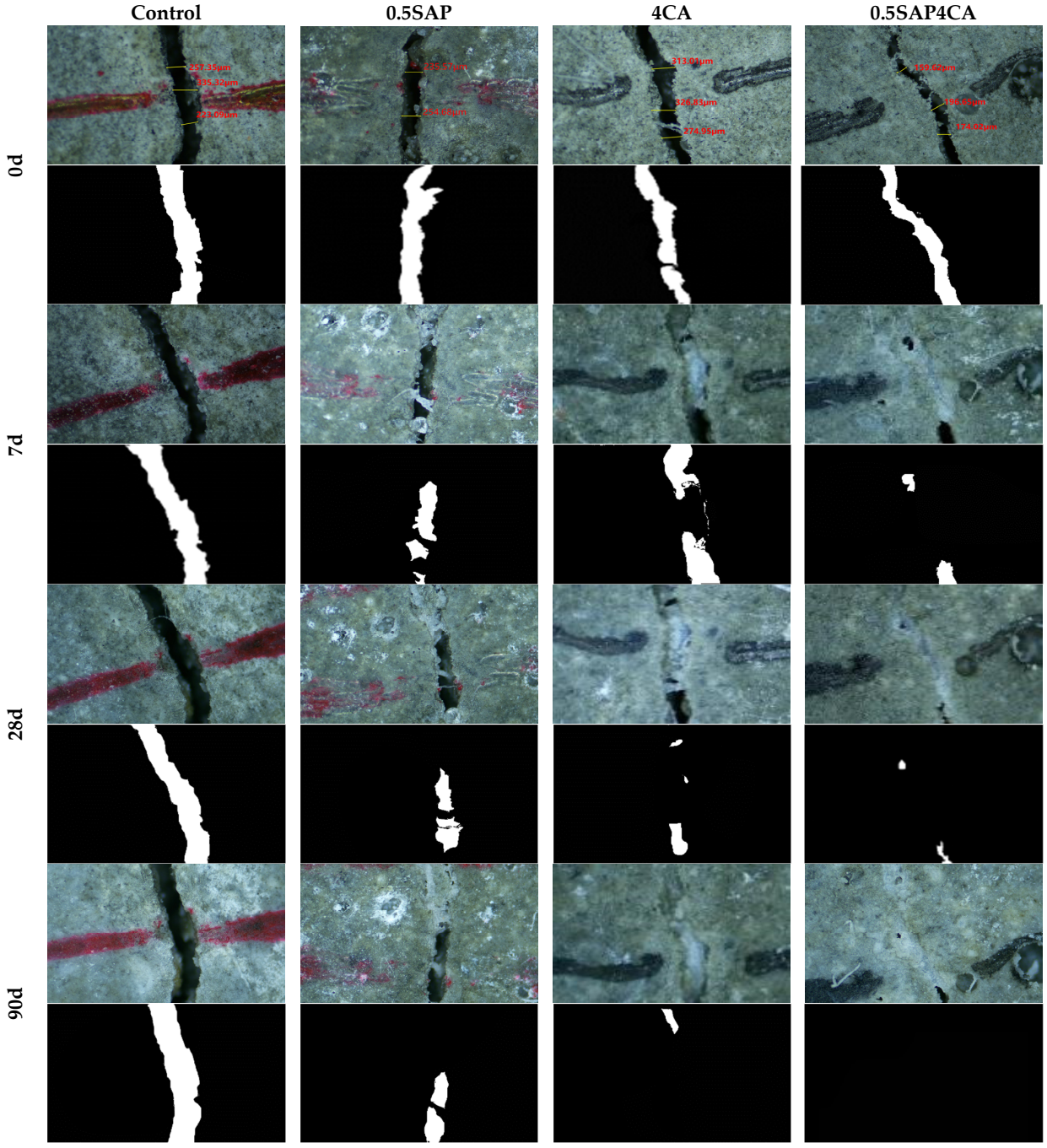

Figure 8. Microscopic observation of mortar self-healing at 0, 7, 28, and 90 days.

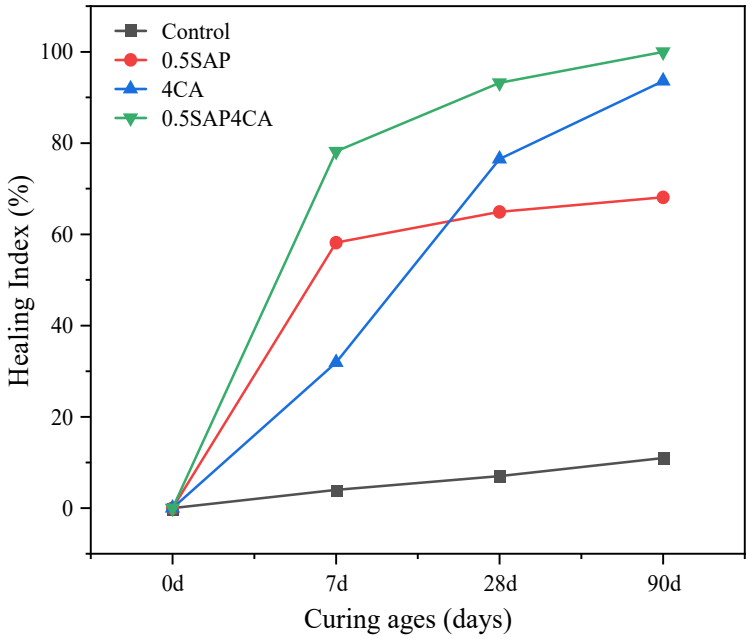

Figure 9. Crack healing index of specimens at 0, 7, 28, and 90 days of healing age.

Table 3. Healing index at 0 d, 7 d, 28 d, and 90 d healing age for each group of specimens.

Group	Healing Index (%)			
	0 d	**7 d**	**28 d**	**90 d**
Control	0	4.0	7.0	11
0.5SAP	0	58.2	64.6	68.1
4CA	0	31.9	76.5	93.6
0.5SAP4CA	0	78.2	93.2	100

The healing index in the 4CA specimens shows a significant increase at 28 days of healing age, and the healing index is 76.5% at 28 d, which is 140% higher than that at 7 d. Due to the addition of the CA in the 4CA specimens, the active substance in the CA continuously reacts with cement hydration products to generate calcium silicate hydrate to fill the cracks [2,42]. The crack healing index of 0.5SAP specimens shows a flat curve, and the healing index was 64.6% at 28 d of healing age, almost the same as that at 7 d of healing. Because the SAP in the cracks swells almost entirely and fills the cracks at the early healing age. The SAP almost stops drinking water and swelling at a later age. For the 0.5SAP4CA specimens, although the healing index is not as high as that of the 4CA specimens, it still exhibits the best healing index at 28 days, reaching a final value of 93.2%. This is because, in the early age, the water absorbed by the SAP is partially released, and the released water promotes the activation reaction between the active substances in the CA and the cement hydration products, forming more hydrated calcium silicate, which results in a reduced amount of the CA available for a reaction in the later age, ultimately showing a lower healing index. Nevertheless, due to the internal curing effect of SAPs, the release of water from the SAP promotes the activation reaction of the remaining CA, thereby increasing the crack healing index.

The healing index at 28 d to 90 d for each group of specimens observed in Figure 9 showed that healing index were almost unchanged for the 0.5SAP specimens, with the healing of cracks due to SAP expansion, as discussed earlier, nearly completing the filling action at an early age. For the 0.5SAP4CA specimens, the healing index continues to rise, as the water absorbed by the SAP in 0.5SAP4CA plays a certain role in promoting the CA activation reaction, leading to an increase in the healing index. Additionally, the healing index of the 0.5SAP4CA specimens is lower than that of the 4CA specimens, as previously

discussed, because the water released by the SAP added to 0.5SAP4CA in the early age promotes the CA reaction, resulting in an insufficient amount of the CA available for a reaction in the later age, showing a reduced rate. However, the water absorbed by the SAP is released, allowing the remaining CA to continue reacting, thus the healing effect continues, showing the best healing effect at the 90-day healing age.

In conclusion, both SAPs and CAs can repair mortar cracks. The physical filling effect of SAPs is almost completed to repair cracks before the 7-day healing age due to the water absorption and swelling of SAPs into an insoluble gel. However, SAPs have little contribution to the healing of cracks after the 7-day healing age. Compared to the physical filling effect of SAPs, the chemical interaction between CAs and CH to form calcium silicate hydrated to seal the cracks takes a longer time to achieve the healing effect. When SAPs and CAs are mixed into the mortar, the mortar shows superior healing ability at an early stage due to the combined effect of early physical filling and internal curing of SAPs and the activation reaction of CAs. Finally, with the release of water in the SAP, the CA reaction is continuously promoted, showing a sustained healing effect.

3.2. Compressive Strength

The compressive strength of mortar at 3, 7, and 28 days is shown in Figure 10. The experimental results indicate that, with the extension of the curing age, the compressive strength of mortar specimens in each group gradually increases, primarily due to the continuous hydration of cement. At curing ages of 3, 7, and 28 days, the compressive strength of the control group specimens is 22.4 MPa, 32.7 MPa, and 48.8 MPa, respectively. In comparison to the control group, the compressive strength of mortar with 0.5 wt.% SAP (0.5SAP specimen) at 3, 7, and 28 days is 20.2 MPa, 28.2 MPa, and 46.1 MPa, respectively, representing a decrease of 9.8%, 13.8%, and 5.5%, respectively. It is evident that the addition of the SAP reduces the compressive strength at all curing ages. The negative impact on compressive strength is attributed to the water absorption and expansion of the SAP, creating larger voids in the mortar. Lee et al. [26] reported that the voids formed by the initial irregularities of the SAP are classified as large pores (diameter greater than 50 nm). Specimens with 4 wt.% CA (4CA specimen) exhibit compressive strengths of 26.4 MPa, 40.1 MPa, and 60.1 MPa at curing ages of 3, 7, and 28 days, respectively. At the 28-day curing age, the compressive strength increases by 23.2%, with increases of 17.9% and 22.6% at 3 and 7 days, respectively. This is attributed to the reactive substances in the CA reacting with the cement hydration product $Ca(OH)_2$, generating dense hydrated calcium silicate to fill the pores in the mortar, ultimately leading to a continuous increase in compressive strength. The compressive strength of the 0.5SAP4CA specimen at 3, 7, and 28 days is 23.6 MPa, 33.1 MPa, and 53.3 MPa, respectively, which is similar to the compressive strength of the control group specimens. This is because the addition of the SAP increases the number of large pores, negatively affecting the compressive strength. However, the CA has a positive effect on compressive strength. In summary, the compressive strength of the 0.5SAP4CA specimen is similar to that of the control group due to the combined action of the CA and the SAP.

3.3. Compressive Strength Recovery

An evaluation of the compressive strength recovery of test specimens reveals the recovery situation. The compressive strength recovery rate is calculated by Equation (2), and the recovery rate is shown in Figure 11. From the figure, it can be seen that the compressive strength recovery rate of the control group specimen is 78.51%, and that of the 0.5SAP specimen is similar, both at 82%. The healing of cracks in the 0.5SAP specimen can be attributed to the secondary hydration of unhydrated cement particles and the physical filling of gaps by SAP water absorption and expansion. However, secondary hydration is limited, and more crack healing is due to the material filling effect. Therefore, compared to the control specimen, the compressive strength recovery rate of the 0.5SAP specimen does not show a significant change. For the 4CA specimen, the compressive strength recovery

rate significantly increases, reaching a final value of 93.98%. One significant reason is that the activation reaction products in the CA fill the cracks, leading to a substantial increase in the compressive strength recovery rate of the specimen. The compressive strength recovery rate of the 0.5SAP4CA specimen is 88.74%, higher than that of the control group and 0.5SAP specimens, but 5.24% lower than that of the 4CA specimen. The 0.5SAP4CA specimen incorporates fillers generated by CA activation reaction. However, since the SAP substitutes for some cement particles, the relative reduction in cement content in the 0.5SAP4CA specimen results in a decreased final compressive strength recovery rate.

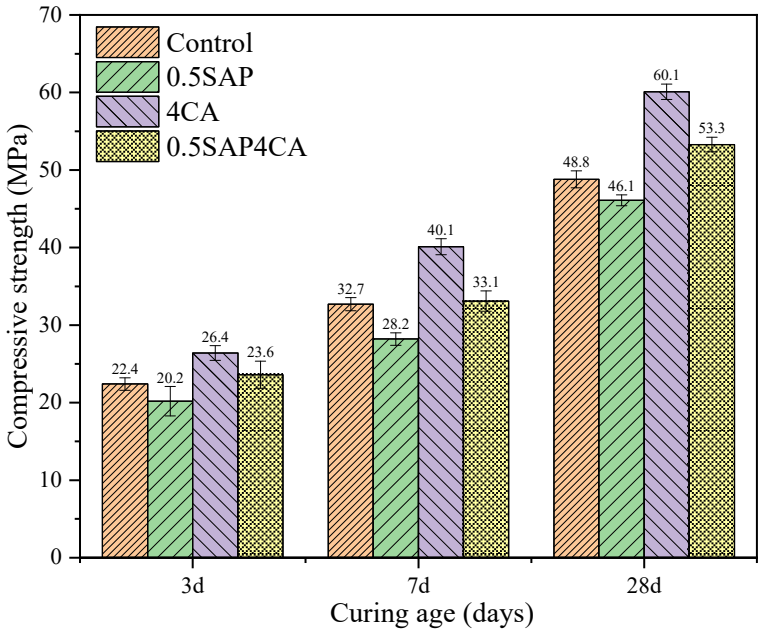

Figure 10. Compressive strength of mortar at 3, 7, and 28 days of curing age.

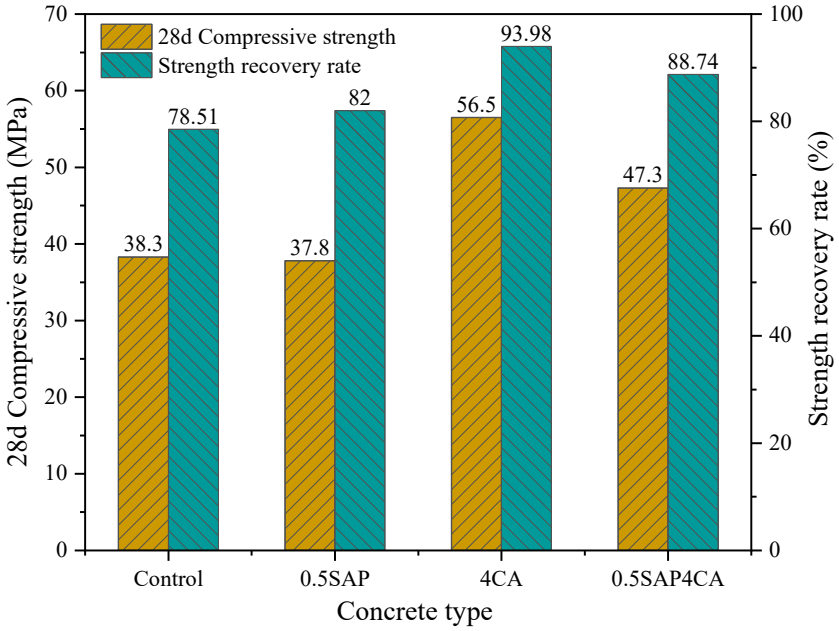

Figure 11. Compressive strength and strength recovery rate of mortar at 28 d.

3.4. Water Absorption Rate

Water absorption can be used to evaluate the healing ability of cracks in cement mortar specimens [43]. To study the healing ability of the specimens, the 28 days water absorption

rate of specimens was tested in this study, and the measured water absorption rates were shown in Figure 12. The experimental results showed that the water absorption heights of 0.5SAP, 4CA, and 0.5SAP4CA specimens were smaller than that of the Control specimens, which indicated that the water absorption rate of all three groups was lower than that of the Control specimens. The water absorption rate of 0.5SAP specimens was lower than that of Control specimens, on the one hand, because the addition of the SAP in the specimens increased the porosity inside the specimens leading to the increase of water absorption rate of the specimens. On the other hand, it was due to the formation of the insoluble gel after the water absorption and swelling of the SAP, and this gel filled the cracks, leading to the decrease of water absorption rate of the specimens. In this study, due to crack healing in the specimens being more pronounced than the effect of reducing water absorption due to the porosity change of the concrete [44], the 0.5SAP specimens showed a decrease in water absorption, with 58.2% at 28 d healing age. And the water absorption of the 4CA and 0.5SAP4CA specimens was lower than the 0.5SAP specimens due to the better healing effect. As shown in Figure 9, the healing index of 4CA and 0.5SAP4CA specimens at 28 d healing age were 76.5% and 93.2%, respectively. Although the 4CA and 0.5SAP4CA specimens had a significant difference in healing index, the water absorption rate of the two specimens was similar. This is mainly because the water absorption rate of the specimens is affected by the healing effect of the cracks in the specimens but also by the specimen's pores. Active substances in the CA react with cement hydration products to produce hydrated calcium silicate to fill the cracks. At the same time, the water absorption and expansion of the SAP cause an increase in concrete porosity. Therefore, when the SAP was introduced into the cement matrix with the CA (0.5SAP4CA specimens), it had a positive effect on the self-healing of the specimens because of the combined effect of early physical filling and internal curing of the SAP and the activation reaction of the CA (η0.5SAP4CA = 93.2%). In addition, due to the increase of the specimen porosity caused by the water absorption and swelling of SAP, the 0.5SAP4CA and 4CA specimens eventually showed similar water absorption rates.

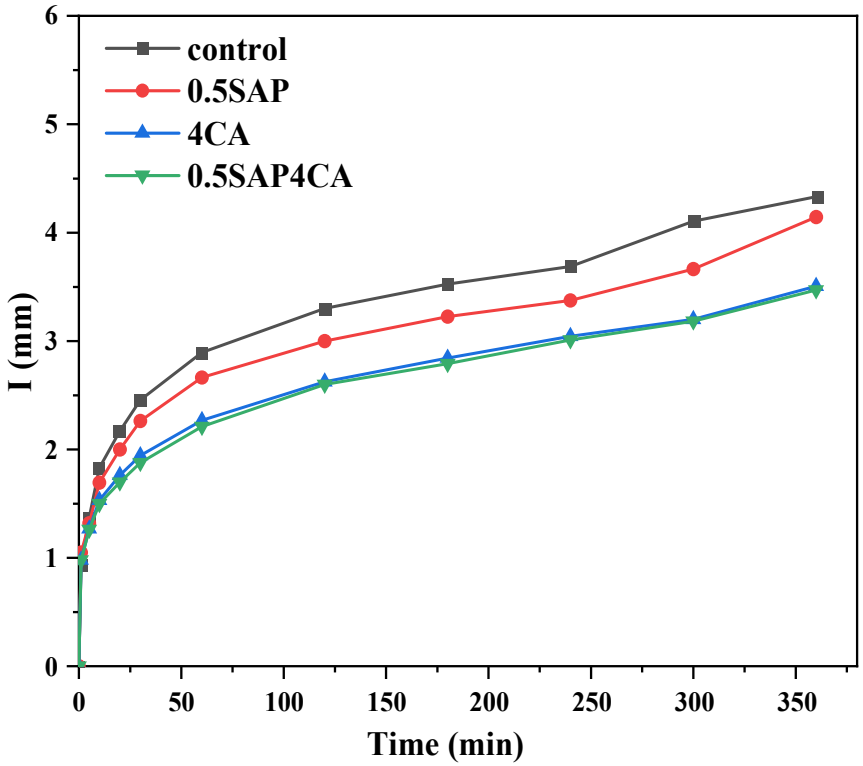

Figure 12. Results of water absorption tests on 28-day healed specimens.

3.5. Micro-Analysis

3.5.1. SEM-EDS Test

The SEM test was used to observe features of the morphology of fillers in cracks of specimens, and the EDS test was used for elemental analysis of the healing products. Figure 13a–d represent SEM images and EDS test results of the Control, 0.5SAP, 4CA, and 0.5SAP4CA samples, respectively. From the SEM image of the Control sample, clustered structures are observed, and EDS elemental analysis reveals a Ca/Si ratio of 0.84, confirming these clustered fillers as C-S-H. The formation of this substance is attributed to the hydration reaction of cement in concrete, consistent with the morphology of C-S-H observed in the study by Huang et al. [45]. Zhu et al. [46] through EDS elemental analysis, found that the Ca/Si ratio of C-S-H generated by cement hydration was 0.89, similar to the Ca/Si ratio of the observed clustered C-S-H structures in this study. In the 0.5SAP specimen, SEM images reveal the generation of numerous hexagonal plate-like $Ca(OH)_2$ around the SAP. This is primarily due to the SAP absorbing some free water during the mixing process. As cement hydration occurs, the water absorbed by the SAP is released, promoting the hydration reaction of the surrounding cement and resulting in the substantial production of $Ca(OH)_2$ around the SAP shell. This phenomenon was confirmed in XRD tests. In addition, on the surface of the SAP shell, similar clustered amorphous C-S-H structures, as observed in the Control sample, were found. EDS elemental analysis indicates a Ca/Si ratio of 0.87, confirming that the C-S-H in both groups of samples originates from the hydration reaction of cement.

Through SEM analysis of the 4CA samples, a significant presence of needle-like structures was observed. Elemental analysis by EDS revealed a Ca/Si ratio of 1.3 in these needle-like structures. Research by Hu et al. [42] confirmed these structures to be C-S-H. The increase in Ca/Si ratio altered the morphological characteristics of C-S-H from amorphous clustered structures to needle-like structures [47]. The abundance of needle-like C-S-H in the 4CA samples may be attributed to the addition of calcium oxide (CaO) in the CA, leading to an elevated Ca/Si ratio. This phenomenon arises because the introduction of the CA ensures a sufficient CaO content, thereby increasing the Ca/Si ratio. Ultimately, the morphology of C-S-H transforms from amorphous clustered structures to needle-like structures. A study by Richardson [48] also confirmed that an increase in Ca/Si ratio results in the transformation of the C-S-H morphology from amorphous clustered structures to needle-like structures. As described in textbooks [49], the morphology of ettringite is typically rod-shaped, while the morphology of C-S-H is amorphous and cluster-like. Interestingly, in this study, an amorphous needle-like structure of C-S-H was observed, causing a transition of C-S-H from the amorphous clustered structure to a needle-like structure because of variations in the Ca/Si ratio. This phenomenon is consistent with the conclusions of Shen et al. [50]. Additionally, it is difficult to find a large number of rod-like ettringite crystals in the cement matrix when the curing age exceeds 28 days [51]. In summary, the needle-like substance discovered in this study is identified as C-S-H. Upon adding 0.5% SAP to the 4CA sample (0.5SAP4CA sample), SEM images revealed the growth of denser needle-like structures within the SAP, eventually penetrating the SAP shell and filling the internal space. This is attributed to the significant increase in needle-like C-S-H structures due to the SAP addition, with two primary causes for this phenomenon. Firstly, as the cement hydration reaction proceeds, water absorbed by the SAP is released, promoting the activation of the CA. Secondly, the water released by the SAP enhances cement hydration, producing more $Ca(OH)_2$. The $Ca(OH)_2$ reacts with the silicon in the CA, generating more C-S-H [52]. Elemental analysis by EDS indicated a Ca/Si ratio of 1.57 in C-S-H.

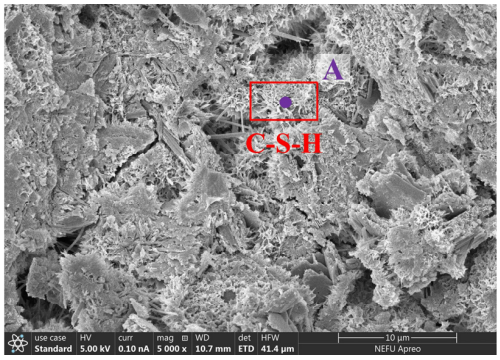

Element	Wt. %	At %
C	8.54	14.22
Ca	20.62	10.29
O	46.55	58.19
Si	24.29	17.3

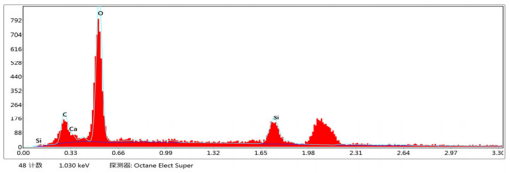

(**a**)

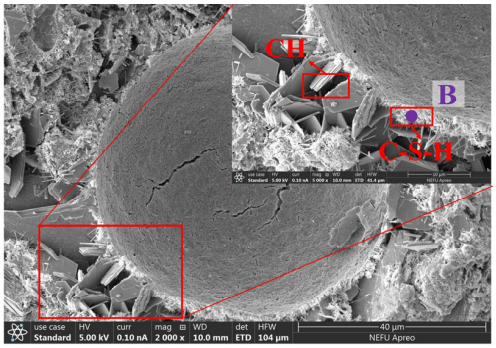

Element	Wt. %	At %
C	8.74	14.16
Ca	18.94	9.2
O	50.6	61.58
Si	21.72	15.06

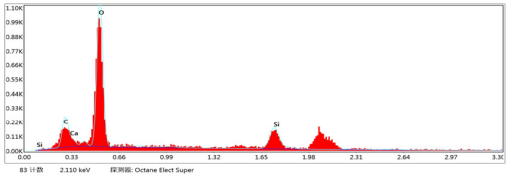

(**b**)

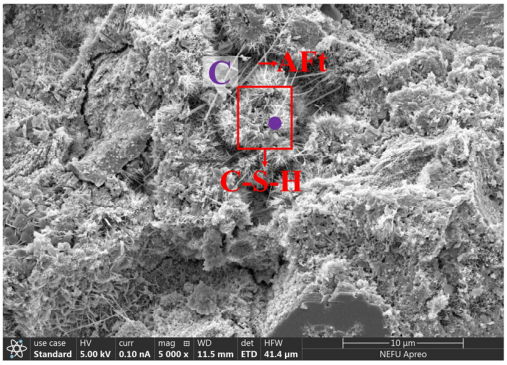

Element	Wt. %	At %
C	11.27	17.73
Ca	20.43	9.63
O	52.53	62.03
Si	15.77	10.61

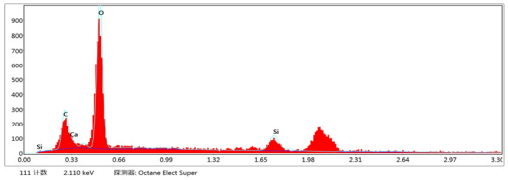

(**c**)

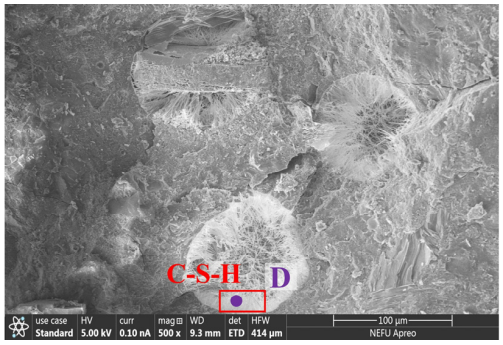

Element	Wt. %	At %
C	5.8	16.63
Ca	10.08	8.65
O	26.92	57.89
Si	6.42	7.87

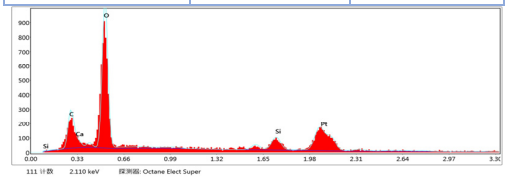

(**d**)

Figure 13. SEM-EDS observation: (**a**) SEM-EDS results of Control: SEM image of healing fillers and EDS energy spectrum of point A; (**b**) SEM-EDS results of 0.5SAP: SEM image of healing fillers and EDS energy spectrum of point B; (**c**) SEM-EDS results of 4CA: SEM image of healing fillers and EDS energy spectrum of point C; and (**d**) SEM-EDS results of 0.5SAP4CA: SEM image of healing fillers and EDS energy spectrum of point D.

3.5.2. X-ray Diffraction

The characteristic peaks of the fillers in all sample cracking areas were analyzed using XRD. The XRD spectra of each group of samples at a healing age of 28 days are shown in Figure 14. Characteristic peaks of $Ca(OH)_2$ can be observed at 2θ values of 18.00°, 34.10°, 42.63°, and 50.81°. Characteristic peaks of C-S-H can be observed at 2θ values of 29.71° and 39.53° [53,54]. Compared to the control group, the characteristic peaks of $Ca(OH)_2$ in the 0.5SAP samples are higher. This is because the SAP gradually releases absorbed moisture during the cement hydration process, promoting the hydration reaction of cement and generating more $Ca(OH)_2$. SEM analysis further revealed an increased quantity of $Ca(OH)_2$ crystals. In contrast, the intensity of the characteristic peaks of $Ca(OH)_2$ in the 4CA samples is lower compared to the control group. This is because the introduction of the CA increases more reactive silicon materials to consume calcium hydroxide, ultimately reducing the quantity of $Ca(OH)_2$. Additionally, it was observed that the production of C-S-H in the 4CA samples enhanced the intensity of its characteristic diffraction peaks at 2θ values of 29.71° and 39.53°. After adding the SAP, the characteristic peaks of C-S-H in the 0.5SAP4CA samples are significantly enhanced. This is mainly because the water released by the SAP promotes the hydration of cement, subsequently generating more $Ca(OH)_2$, providing additional reactants for the CA reaction. Furthermore, it was found that the water released by the SAP enhances the activation of the CA, and SEM testing confirms that the water released by the SAP promotes the generation of more C-S-H. These findings are consistent with the observations of Oliveira [55] and Zhang [56] et al.

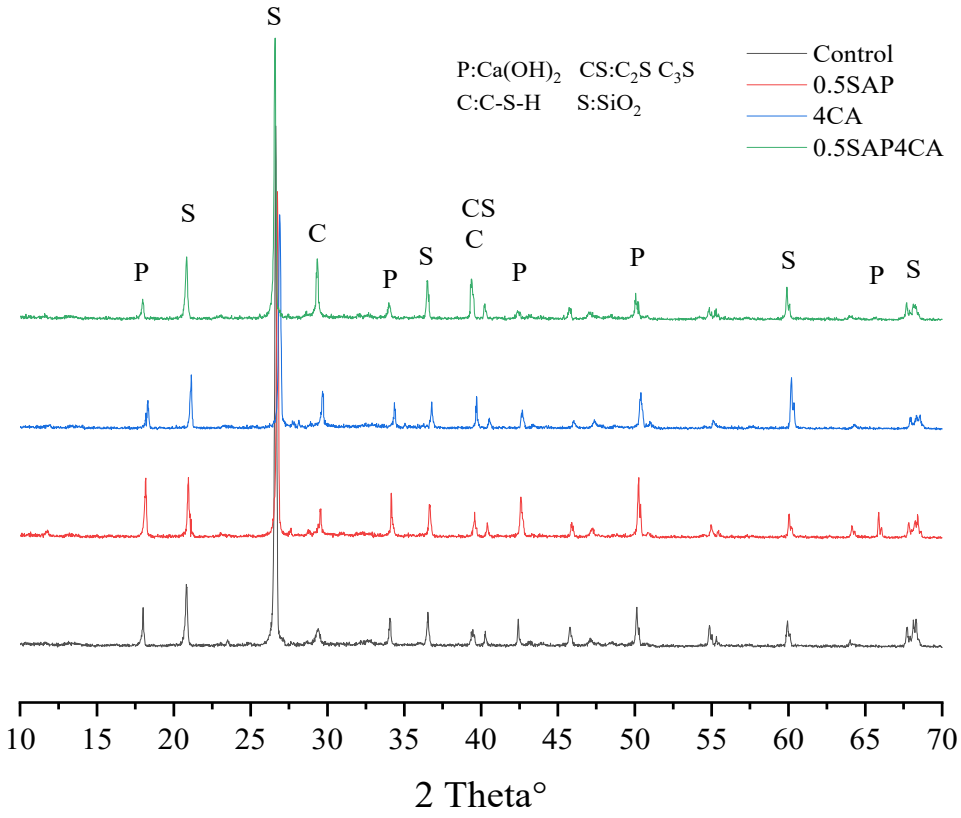

Figure 14. XRD test results of specimens at 28 d of healing age.

4. Conclusions

This research examined the implications of integrating SAPs and CAs on the self-healing performance of mortar. Through experimental evaluations and data interpretation, the ensuing conclusions were derived:

(1) It can be found that both the physical filling effect of SAP water absorption and expansion and the chemical interaction of the CA activation reaction can effectively repair

mortar cracks by observing the crack healing through an optical microscope. The physical filling effect of the SAP almost completed the healing effect before the 7-day healing age, and the recovery of cracks was fragile after the 7-day healing age. Compared with the SAP physical filling effect, the CA blend still has the ability to repair at 90 d of healing age. In addition, the activation reaction of the CA was influenced by water. When SAPs and CAs were incorporated into mortar matrix, the mortar showed best healing ability before the 7-day healing age due to early physical filling and internal curing of the SAP and activation reaction of the CA.

(2) Compared to Control specimens, the introduction of SAPs decreased compressive strength of mortar. Incorporating CAs resulted in an increase in the strength of specimens, because the activation reaction of CAs, which ultimately produces dense hydrated calcium silicate structure, increases compressive strength.

(3) The recovery rate was 78.51% for Control specimens and 82% for the 0.5 SAP specimens. It was confirmed that the contribution of continuous hydration and the physical filling of SAPs in the recovery of strength was limited. The incorporation of CAs in mortar specimens resulted in a recovery rate of 93.98%. This outcome attests to the remarkable efficacy of CAs' activation reaction in generating calcium silicate hydrated and filling cracks, thereby facilitating restoration of compressive strength.

(4) When SAPs were introduced into the cement matrix with CAs, the positive impact on self-healing of specimens because of combined effect of early physical filling and internal curing effect of SAPs and the activation reaction of CAs. In addition, SAPs will increase the porosity of the specimen. The 0.5SAP4CA and 4CA specimens eventually showed similar water absorption rates.

(5) By SEM-EDS tests for the healing products, the presence of C-S-H with a clustered structure was identified in both the Control and 0.5SAP specimens. This confirmed that C-S-H in both groups of samples was from the cement hydration reaction. Numerous needle-like C-S-H was observed for the 4CA specimens and Ca/Si value was 1.3. It has been found that CA increased the Ca/Si value, and C-S-H changed from an amorphous cluster structure to a needle-like structure. This needle-like structure C-S-H can be observed in 0.5SAP4CA specimens to penetrate the SAP shell and occupy the internal space of the SAP.

(6) The XRD test results indicate that compared to Control specimens, the 0.5SAP specimens have a higher intensity of $Ca(OH)_2$ due to SAP internal curing. The 4CA specimens demonstrate an enhanced intensity of C-S-H, a consequence of CA incorporation. The 0.5SAP4CA specimens manifest an elevated presence of $Ca(OH)_2$, stemming from the SAP internal curing mechanism, which provides more $Ca(OH)_2$ reactants for the reaction of the CA. In addition, water released from the SAP promoted the activation reaction of the CA. Therefore, there was a significant enhancement in the C-S-H characteristic peak in 0.5SAP4CA specimen.

5. Limitations and Future Work

Although the synergistic effect of SAPs and CAs can completely repair cracks at the healing age of 90 d, there are still several aspects that need to be improved. In order to get the impact of CAs' activation reaction on the self-healing performance of cracks, consider removing the effect of SAPs on the activation reaction of CAs in the final crack healing effect in future research. In addition, future research needs to consider the economic and environmental feasibility of these materials to promote their widespread application in the industrial and construction fields.

Author Contributions: G.-Z.Z.: conceptualization, methodology, investigation, supervision, and writing—review and editing. X.M.: methodology, data curation, and writing—review and editing. Y.L.: conceptualization, supervision, validation, resources, project administration, funding acquisition, and writing—review. All authors have read and agreed to the published version of the manuscript.

Funding: This research was financially supported by the Analysis and Testing Center of Northeast Forestry University; Fundamental Research Funds for the Central Universities Science (No. 2572022DX10).

Data Availability Statement: The data presented in this study are available on request from the corresponding author. The data are not publicly available due to privacy.

Conflicts of Interest: The authors declare no conflict of interest.

References

1. Chindasiriphan, P.; Yokota, H.; Pimpakan, P. Effect of fly ash and superabsorbent polymer on concrete self-healing ability. *Constr. Build. Mater.* **2020**, *233*, 116975. [CrossRef]
2. Reddy, C.; Ramesh, B.M.K.; Macrin, D. Effect of crystalline admixtures, polymers and fibers on self-healing concrete—A review. *Mater. Today Proc.* **2020**, *33*, 763–770. [CrossRef]
3. Tang, Q.; Hu, J.; Yu, T. Electromagnetic evaluation of brick specimens using synthetic aperture radar imaging. *NDT E Int.* **2019**, *104*, 98–107. [CrossRef]
4. Snoeck, D.; Debo, J.; De Belie, N. Translucent self-healing cementitious materials using glass fibers and superabsorbent polymers. *Dev. Built Environ.* **2020**, *3*, 100012. [CrossRef]
5. Du, W.; Lin, R.; Liu, Q. Investigation of isophorone diisocyanate microcapsules to improve self-healing properties and sulfate resistance of concrete. *Constr. Build. Mater.* **2021**, *300*, 124438. [CrossRef]
6. Li, Y.; Yu, J.; Cao, Z.; He, P.; Liu, Q.; Han, X.; Wan, Y. Preparation and application of novel microcapsules ruptured by microwave for self-healing concrete. *Constr. Build. Mater.* **2021**, *304*, 124616. [CrossRef]
7. Feng, J.; Chen, B.; Sun, W.; Wang, Y. Microbial induced calcium carbonate precipitation study using Bacillus subtilis with application to self-healing concrete preparation and characterization. *Constr. Build. Mater.* **2021**, *280*, 122460. [CrossRef]
8. Algaifi, H.A.; Bakar, S.A.; Sam, A.R.M.; Abidin, A.R.Z.; Shahir, S.; Al-Towayti, W.A.H. Numerical modeling for crack self-healing concrete by microbial calcium carbonate. *Constr. Build. Mater.* **2018**, *189*, 816–824. [CrossRef]
9. Tan, L.; Ke, X.; Li, Q.; Gebhard, S.; Ferrandiz-Mas, V.; Paine, K.; Chen, W. The effects of biomineralization on the localised phase and microstructure evolutions of bacteria-based self-healing cementitious composites. *Cem. Concr. Compos.* **2022**, *128*, 104421. [CrossRef]
10. Chen, W.; Feng, K.; Wang, Y.; Lin, Y.; Qian, H. Evaluation of self-healing performance of a smart composite material (SMA-ECC). *Constr. Build. Mater.* **2021**, *290*, 123216. [CrossRef]
11. Chen, W.; Lin, B.; Feng, K.; Cui, S.; Zhang, D. Effect of shape memory alloy fiber content and preloading level on the self-healing properties of smart cementitious composite (SMA-ECC). *Constr. Build. Mater.* **2022**, *341*, 127797. [CrossRef]
12. Al-Kheetan, M.J.; Rahman, M.M.; Chamberlain, D.A. A novel approach of introducing crystalline protection material and curing agent in fresh concrete for enhancing hydrophobicity. *Constr. Build. Mater.* **2018**, *160*, 644–652. [CrossRef]
13. Azarsa, P.; Gupta, R.; Biparva, A. Assessment of self-healing and durability parameters of concretes incorporating crystalline admixtures and Portland Limestone Cement. *Cem. Concr. Compos.* **2019**, *99*, 17–31. [CrossRef]
14. Sisomphon, K.; Copuroglu, O.; Koenders, E.A.B. Self-healing of surface cracks in mortars with expansive additive and crystalline additive. *Cem. Concr. Compos.* **2012**, *34*, 566–574. [CrossRef]
15. Hu, X.; Xiao, J.; Zhang, Z.; Wang, C.; Long, C.; Dai, L. Effects of CCCW on properties of cement-based materials. A review. *J. Build. Eng.* **2022**, *50*, 104184. [CrossRef]
16. Park, B.; Choi, Y.C. Self-healing capability of cementitious materials with crystalline admixtures and super absorbent polymers (SAPs). *Constr. Build. Mater.* **2018**, *189*, 1054–1066. [CrossRef]
17. Roig-Flores, M.; Moscato, S.; Serna, P.; Ferrara, L. Self-healing capability of concrete with crystalline admixtures in different environments. *Constr. Build. Mater.* **2015**, *86*, 1–11. [CrossRef]
18. Kazemian, M.; Shafei, B. Internal curing capabilities of natural zeolite to improve the hydration of ultra-high performance concrete. *Constr. Build. Mater.* **2022**, *340*, 127452. [CrossRef]
19. Liu, J.; Liu, G.; Zhang, W.; Li, Z.; Xing, F.; Tang, L. Application potential analysis of biochar as a carbon capture material in cementitious composites. A review. *Constr. Build. Mater.* **2022**, *350*, 128715. [CrossRef]
20. Yang, J.; Guo, Y.; Shen, A.; Chen, Z.; Qin, X.; Zhao, M. Research on drying shrinkage deformation and cracking risk of pavement concrete internally cured by SAPs. *Constr. Build. Mater.* **2019**, *227*, 116705. [CrossRef]
21. Yao, Y.; Zhu, Y.; Yang, Y. Incorporation superabsorbent polymer (SAP) particles as controlling pre-existing flaws to improve the performance of engineered cementitious composites (ECC). *Constr. Build. Mater.* **2012**, *28*, 139–145. [CrossRef]
22. Assmann, A.; Reinhardt, H.W. Tensile creep and shrinkage of SAP modified concrete. *Cem. Concr. Res.* **2014**, *58*, 179–185. [CrossRef]
23. Mechtcherine, V.; Secrieru, E.; Schröfl, C. Effect of superabsorbent polymers (SAPs) on rheological properties of fresh cement-based mortars—Development of yield stress and plastic viscosity over time. *Cem. Concr. Res.* **2015**, *67*, 52–65. [CrossRef]
24. Craeye, B.; Geirnaert, M.; Schutter, G.D. Super absorbing polymers as an internal curing agent for mitigation of early-age cracking of high-performance concrete bridge decks. *Constr. Build. Mater.* **2011**, *25*, 1–13. [CrossRef]
25. Kanellopoulou, I.; Karaxi, E.K.; Karatza, A.; Kartsonakis, I.A.; Charitidis, C.A. Effect of submicron admixtures on mechanical and self-healing properties of cement-based composites. *Fatigue Fract. Eng. Mater. Struct.* **2019**, *42*, 1494–1509. [CrossRef]
26. Lee, H.X.D.; Wong, H.S.; Buenfeld, N.R. Self-sealing of cracks in concrete using superabsorbent polymers. *Cem. Concr. Res.* **2016**, *79*, 194–208. [CrossRef]

27. Snoeck, D.; Dewanckele, J.; Cnudde, V.; De Belie, N. X-ray computed microtomography to study autogenous healing of cementitious materials promoted by superabsorbent polymers. *Cem. Concr. Compos.* **2016**, *65*, 83–93. [CrossRef]
28. Snoeck, D.; Steuperaert, S.; Van Tittelboom, K.; Dubruel, P.; De Belie, N. Visualization of water penetration in cementitious materials with superabsorbent polymers by means of neutron radiography. *Cem. Concr. Res.* **2012**, *42*, 1113–1121. [CrossRef]
29. Al-Kheetan Mazen, J.; Rahman Mujib, M.; Chamberlain Denis, A. Optimum Mix Design for Internally Integrated Concrete with Crystallizing Protective Material. *J. Mater. Civ. Eng.* **2019**, *31*, 04019101. [CrossRef]
30. Shang, X.; Jing, D. The present research and application of cement based permeated crystalline materials. *J. Water Resour. Arch. Eng.* **2015**, *13*, 131–135.
31. Zhang, C.; Lu, R.; Li, Y.; Guan, X. Effect of crystalline admixtures on mechanical, self-healing and transport properties of engineered cementitious composite. *Cem. Concr. Compos.* **2021**, *124*, 104256. [CrossRef]
32. Gruyaert, E.; Debbaut, B.; Snoeck, D.; Díaz, P.; Arizo, A.; Tziviloglou, E.; Schlangen, E.; De Belie, N. Self-healing mortar with pH-sensitive superabsorbent polymers. Testing of the sealing efficiency by water flow tests. *Smart Mater. Struct.* **2016**, *25*, 084007. [CrossRef]
33. Hong, G.; Song, C.; Park, J.; Choi, S. Hysteretic behavior of rapid self-sealing of cracks in cementitious materials incorporating superabsorbent polymers. *Constr. Build. Mater.* **2019**, *195*, 187–197. [CrossRef]
34. Snoeck, D.; Schaubroeck, D.; Dubruel, P.; De Belie, N. Effect of high amounts of superabsorbent polymers and additional water on the workability, microstructure and strength of mortars with a water-to-cement ratio of 0.50. *Constr. Build. Mater.* **2014**, *72*, 148–157. [CrossRef]
35. Wang, X.; Chen, S.; Ren, J.; Huang, R.; Yang, Z.; Wang, W.; Liu, J. Effect of super absorbent polymer and mineral additives on mechanical, shrinkage and healing properties of self-healing lightweight aggregate concrete under different curing regimes. *Constr. Build. Mater.* **2022**, *357*, 129377. [CrossRef]
36. De Souza Oliveira, A.; Filho, R.D.T.; de Moraes Rego Fairbairn, E.; de Oliveira, L.F.C.; da Fonseca Martins Gomes, O. Microstructural characterization of self-healing products in cementitious systems containing crystalline admixture in the short- and long-term. *Cem. Concr. Compos.* **2022**, *126*, 104369. [CrossRef]
37. Cuenca, E.; Tejedor, A.; Ferrara, L. A methodology to assess crack-sealing effectiveness of crystalline admixtures under repeated cracking-healing cycles. *Constr. Build. Mater.* **2018**, *179*, 619–632. [CrossRef]
38. *C109/C109M-21*; Standard Test Method for Compressive Strength of Hydraulic Cement Mortars (Using 2-in. or [50 mm] Cube Specimens). ASTM: West Conshohocken, PA, USA, 2021.
39. Wang, R.; Yu, J.; Gu, S.; He, P.; Han, X.; Liu, Q. Investigation of self-healing capability on surface and internal cracks of cement mortar with ion chelator. *Constr. Build. Mater.* **2020**, *236*, 117598. [CrossRef]
40. *C1585-20*; Standard Test Method for Measurement of Rate of Absorption of Water by Hydraulic Cement Concretes. ASTM: West Conshohocken, PA, USA, 2020.
41. Snoeck, D.; Van den Heede, P.; Van Mullem, T.; De Belie, N. Water penetration through cracks in self-healing cementitious materials with superabsorbent polymers studied by neutron radiography. *Cem. Concr. Res.* **2018**, *113*, 86–98. [CrossRef]
42. Yu, R.; Zhang, X.; Hu, Y.; Li, J.; Zhou, F.; Liu, K.; Zhang, J.; Wang, J.; Shui, Z. Development of a rapid hardening ultra-high performance concrete (R-UHPC): From macro properties to micro structure. *Constr. Build. Mater.* **2022**, *329*, 127188. [CrossRef]
43. Aspiotis, K.; Sotiriadis, K.; Ntaska, A.; Mácová, P.; Badogiannis, E.; Tsivilis, S. Durability assessment of self-healing in ordinary Portland cement concrete containing chemical additives. *Constr. Build. Mater.* **2021**, *305*, 124754. [CrossRef]
44. Jiang, Z.; Li, W.; Yuan, Z. Influence of mineral additives and environmental conditions on the self-healing capabilities of cementitious materials. *Cem. Concr. Compos.* **2015**, *57*, 116–127. [CrossRef]
45. Huang, H.; Ye, G.; Damidot, D. Characterization and quantification of self-healing behaviors of microcracks due to further hydration in cement paste. *Cem. Concr. Res.* **2013**, *52*, 71–81. [CrossRef]
46. Zhu, X.; Tang, D.; Yang, K.; Zhang, Z.; Li, Q.; Pan, Q.; Yang, C. Effect of $Ca(OH)_2$ on shrinkage characteristics and microstructures of alkali-activated slag concrete. *Constr. Build. Mater.* **2018**, *175*, 467–482. [CrossRef]
47. Zhang, Z.; Scherer, G.W.; Bauer, A. Morphology of cementitious material during early hydration. *Cem. Concr. Res.* **2018**, *107*, 85–100. [CrossRef]
48. Richardson, I.G. Tobermorite/jennite- and tobermorite/calcium hydroxide-based models for the structure of C-S-H: Applicability to hardened pastes of tricalcium silicate, β-dicalcium silicate, Portland cement, and blends of Portland cement with blast-furnace slag, metakaolin, or silica fume. *Cem. Concr. Res.* **2004**, *34*, 1733–1777.
49. Mehta, P.K.; Monteiro, P.J. *Concrete: Microstructure, Properties, and Materials*; McGraw-Hill Education: Singapore, 2014.
50. Peng, L.; Jiang, Y.; Ban, J.; Shen, Y.; Ma, Z.; Zhao, Y.; Shen, P.; Poon, C.-S. Mechanism underlying early hydration kinetics of carbonated recycled concrete fines-ordinary portland cement (CRCF-OPC) paste. *Cem. Concr. Compos.* **2023**, *144*, 105275. [CrossRef]
51. Long, W.-J.; Xie, J.; Zhang, X.; Fang, Y.; Khayat, K.H. Hydration and microstructure of calcined hydrotalcite activated high-volume fly ash cementitious composite. *Cem. Concr. Compos.* **2021**, *123*, 104213. [CrossRef]
52. De Souza Oliveira, A.; Dweck, J.; de Moraes Rego Fairbairn, E.; da Fonseca Martins Gomes, O.; Toledo Filho, R.D. Crystalline admixture effects on crystal formation phenomena during cement pastes' hydration. *J. Therm. Anal. Calorim.* **2020**, *139*, 3361–3375. [CrossRef]

53. Wehbe, Y.; Ghahremaninezhad, A. Combined effect of shrinkage reducing admixtures (SRA) and superabsorbent polymers (SAP) on the autogenous shrinkage, hydration and properties of cementitious materials. *Constr. Build. Mater.* **2017**, *138*, 151–162. [CrossRef]
54. Wang, Y.-S.; Lee, H.-S.; Lin, R.-S.; Wang, X.-Y. Effect of silicate-modified calcium oxide-based expansive agent on engineering properties and self-healing of ultra-high-strength concrete. *J. Build. Eng.* **2022**, *50*, 104230. [CrossRef]
55. De Souza Oliveira, A.; da Fonseca Martins Gomes, O.; Ferrara, L.; de Moraes Rego Fairbairn, E.; Toledo Filho, R.D. An overview of a twofold effect of crystalline admixtures in cement-based materials: From permeability-reducers to self-healing stimulators. *J. Build. Eng.* **2021**, *41*, 102400. [CrossRef]
56. Zhang, Y.; Wang, R.; Ding, Z. Influence of Crystalline Admixtures and Their Synergetic Combinations with Other Constituents on Autonomous Healing in Cracked Concrete—A Review. *Materials* **2022**, *15*, 440. [CrossRef]